Virologica Sinica 40 (2025) 439–450

Contents lists available at ScienceDirect

Virologica Sinica

journal homepage: www.keaipublishing.com/en/journals/virologica-sinica
www.virosin.org

Research Article

Eltrombopag, an FDA-approved drug, inhibits dengue virus type 2 by targeting NS2B-NS3 protease

Xuerui Zhu [a], Xiao Gao [a,b], Yan Wu [a], Jia Lu [a,b], Xinlan Chen [a,b], Chenshu Zhao [a], Haoyu Li [a,b], Zhongfa Zhang [a], Shuwen Liu [c], Gengfu Xiao [a,b], Xiaoyan Pan [a,b,*]

[a] State Key Laboratory of Virology and Biosafety, Wuhan Institute of Virology, Chinese Academy of Sciences, Wuhan 430207, China
[b] University of Chinese Academy of Sciences, Beijing 101400, China
[c] School of Pharmaceutical Sciences, Southern Medical University, Guangzhou 510515, China

ARTICLE INFO

Keywords:
Dengue virus type 2 (DENV 2)
Antiviral agent
NS2B-NS3 protease
Eltrombopag
Allosteric inhibitor

ABSTRACT

Dengue viruses (DENV) have spread throughout the world and pose a huge threat to human life. The most widespread serotype is type 2 DENV (DENV 2), which has no specific treatment. NS2B-NS3 protease plays a pivotal role in DENV replication because of its function in cleavage of the viral polyprotein; thus, it is considered a promising target for antiviral discovery. In this study, we developed a high-throughput screening system based on the NS2B-NS3 protease to identify candidates from an FDA-approved drug library. Eltrombopag was screened out of 3273 drugs, and demonstrated inhibition on DENV 2 at the micromolar level *in vitro,* significantly reducing viral loads in the targeted organs of challenged mice following intraperitoneal injection. Further mechanistic analysis showed that eltrombopag allosterically binds to the DENV 2 NS2B-NS3 protease in a reversible, non-competitive manner, therefore inhibiting DENV 2 at the post-infection stage. In addition, eltrombopag inhibited the NS2B-NS3 proteases of DENV 4 and Zika virus, suggesting its potential as a broad-spectrum antiviral agent. This study repurposed eltrombopag as a promising antiviral agent against DENV, providing an alternative for antiviral development against flaviviruses.

INTRODUCTION

Owing to animal migration, climate change, urbanization, and international tourism, flavivirus infections have become endemic worldwide, posing a huge threat to human health (Weaver and Reisen, 2010; Imperato, 2016). Among the mosquito-borne flaviviruses, which include West Nile virus, yellow fever virus, dengue virus (DENV), Zika virus (ZIKV), and Japanese encephalitis virus, DENV, especially serotype 2 (DENV 2), is the most widespread (Niu et al., 2020). DENV 2 leads to approximately 100 million symptomatic infections and more than 10,000 deaths each year in more than 100 tropical and subtropical nations (Bhatt et al., 2013; Messina et al., 2019), representing an increase of 65.5% since 2007 (Murray et al., 2013; Paz-Bailey et al., 2024). Although the major symptoms of primary DENV infection are fever, headache, muscle or bone pain, and rash, many severe dengue symptoms, such as petechial bleeding, plasma leakage, and even death, are caused by secondary infections, which are attributed to antibody-dependent enhancement (Katzelnick et al., 2017; Narayan and Tripathi, 2020). Similarly, ZIKV originated in Brazil and spread exponentially in the Americas, giving rise to one of the most severe epidemics of this century owing to its association with adverse fetal outcomes and Guillain–Barré syndrome (Shukla et al., 2016; Saron et al., 2023). Although several dengue vaccines have been approved in endemic areas or tested in clinical trials (World Health Organization, 2017; Wilder-Smith et al., 2019), no dedicated therapeutic agents specifically target DENV or ZIKV, with supportive care representing the mainstay of treatment. Therefore, the development of effective strategies and medications for the treatment of DENV and mosquito-borne flaviviruses represents a pressing challenge that demands immediate attention (Lim, 2019; Feng, 2024).

Flaviviruses such as DENV and ZIKV are single-stranded, positive-sense RNA viruses with a genome length of approximately 11 kb. The polyproteins produced during viral proliferation are immediately cleaved by host and viral-encoded proteases, resulting in the production of three structural proteins: capsid (C), membrane (prM/M), and envelope (E)

* Corresponding author.
E-mail address: panxy@wh.iov.cn (X. Pan).

https://doi.org/10.1016/j.virs.2025.05.009
Received 19 February 2025; Accepted 26 May 2025
Available online 28 May 2025

proteins, as well as seven nonstructural proteins (NSs): NS1, NS2A, NS2B, NS3, NS4A, NS4B, and NS5. NS proteins are found at the 3′ end of the genome and primarily regulate RNA replication, viral assembly, and host response (Rice et al., 1985). The inhibition of flaviviral NS proteins is key for the development of targeted antiviral medications. Notably, NS3 is a viral NS protein with enzymatic functions that is primarily responsible for catalyzing the hydrolysis and cleavage of polyproteins, especially those active at sites NS2A/NS2B, NS2B/NS3, and NS3/NS4A, which are crucial for supporting viral replication (Patkar and Kuhn, 2008). NS3 activation is contingent upon participation of the co-factor NS2B (Luo et al., 2015). Therefore, NS2B-NS3 protease (NS2B-NS3pro) is an attractive target for antiviral drug discovery (Starvaggi et al., 2024).

In this study, we established a high-throughput screening system by targeting NS2B-NS3pro using fluorescence resonance energy transfer (FRET) assay. By repurposing a library of 3273 FDA-approved drugs, we show that eltrombopag, a thrombopoietin receptor agonist and iron chelator that increases platelet counts in patients with chronic immune thrombocytopenia (Zhang and Kolesar, 2011; Vlachodimitropoulou et al., 2017), exerts inhibitory effects against NS2B-NS3pro and DENV 2 infection both *in vitro* and *in vivo*. We also demonstrated the broad-spectrum inhibition of related flaviviruses, such as ZIKV. The mechanism of action involves non-covalent binding of eltrombopag to the allosteric site of NS3pro, which may interfere with the interaction between NS3pro and its co-factor NS2B or substrate. This study reveals new drug candidates for the treatment of DENV and mosquito-borne flaviviruses.

RESULTS

Screening of DENV 2 NS2B-NS3pro inhibitors from an FDA-approved drug library

For efficient screening of NS2B-NS3pro inhibitors, we established a high-throughput screening system based on a 384-well plate enzyme-substrate reaction and FRET detection. In view of the advantages of the FDA-approved drug library for chemical diversity and safety, we rapidly screened 89 compounds from 3273 drugs that inhibit enzymatic activity by more than 80% at a concentration of 50 μM (Fig. 1A). These compounds were then validated by cellular antiviral assays by both RT-qPCR and indirect immunofluorescence assay (IFA), which revealed eight compounds that inhibit DENV 2 infection by more than 60% at a concentration at 5 μM (Fig. 1B). To further investigate these compounds, we determined their half effective concentration (EC_{50}) and half cytotoxicity concentration (CC_{50}) on both BHK-21 and Huh 7 cells. The results showed that pralatrexate, MK-8742, eltrombopag, GS-5885, and benzamil hydrochloride have selective indexes greater than 100, showing both good efficacy and safety *in vitro* (Table 1). The flow chart of this process is shown in Fig. 1C.

Identification of eltrombopag as a promising therapeutic candidate for DENV 2

Based on these results, pralatrexate, MK-8742, eltrombopag, GS-5885, and benzamil hydrochloride were used for further analysis. As shown in Fig. 2A, the five compounds inhibited DENV 2 infection in a dose-dependent manner but had no obvious cytotoxic effects on the cells. Moreover, the five compounds inhibited NS2B-NS3pro of DENV 2 at μM levels, while only eltrombopag selectively inhibited NS2B-NS3pro in contrast to the human serine protease (Trypsin) (Fig. 2B). To further validate the interaction of the five hit compounds and NS2B-NS3pro, we employed a surface plasmon resonance (SPR) assay to determine binding affinities. Three compounds showed strong binding capacity on NS2B-NS3pro with a $K_D = 5.56$ μM of eltrombopag, whereas pralatrexate and benzamil hydrochloride showed almost no binding affinity (Fig. 2C). Thus, MK-8742, eltrombopag, and GS-5885 were deemed to exhibit antiviral effects against DENV 2 infection through targeting NS2B-NS3pro.

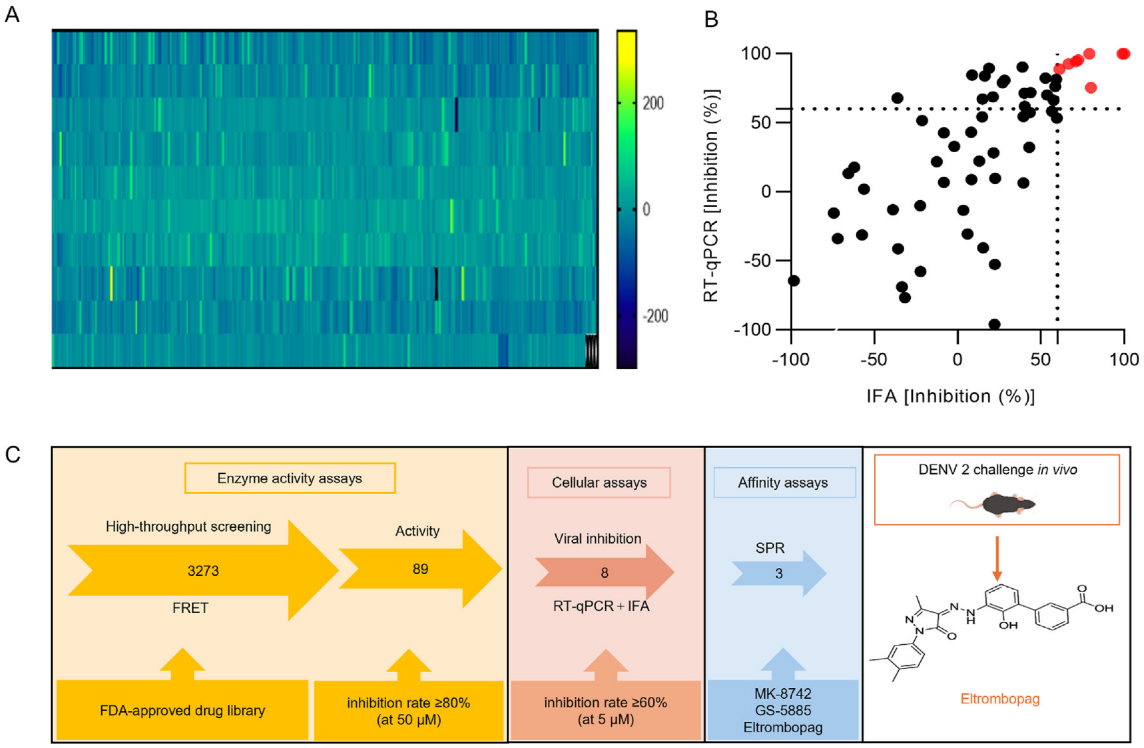

Fig. 1. High-throughput screening of NS2B-NS3pro inhibitors from an FDA-approved library. **A** Heatmap showing the high-throughput screening results of 3723 compounds against NS2B-NS3pro. **B** Compounds with > 60% inhibition of DENV 2 infection at 5 μM on the BHK-21 cell model were detected by RT-qPCR and indirect immunofluorescence assay (IFA). Hit compounds were marked in red. **C** The screening flowchart for screening DENV 2 NS2B-NS3pro inhibitors from the FDA-approved library.

Table 1
Inhibition and cytotoxicities of the hit compounds.

NO.	Compounds	EC_{50} (BHK-21 μM)	EC_{50} (Huh 7 μM)	CC_{50} (BHK-21 μM)	SI (CC_{50}/EC_{50})
1	Pralatrexate	<0.0076	<0.07	104	> 13684.21
2	MK-8742	0.04592	0.1609	>600	> 13066.2
3	Eltrombopag	0.3158	1.46	104.5	330.91
4	GS-5885	3.315	0.5294	>600	> 181
5	Benzamil hydrochloride	0.3679	2.618	44.46	120.85
6	Evans Blue	4.848	0.3374	242.3	49.98
7	AGN190168	10.86	0.107	262.3	24.15
8	MK-870	33.67	8.737	168.6	5.01

Notes: Compounds are listed in order of their selective indexes.

Therefore, these three compounds were subjected to animal experiments to investigate the *in vivo* antiviral efficacy. Adult female AG129 mice exhibiting transient viremia lasting for several days, with peak viral loads at day 2 or 3 post-infection (Baldon et al., 2022), were challenged with DENV 2 via intraperitoneal injection (*i.p.*), and administered MK-8742, eltrombopag, and GS-5885 via intragavage (*i.g.*), with the nucleoside analog, NITD008, used as a positive control (Fig. 2D). Mice were monitored for body weight during the experimental period and sacrificed for tissue harvest two days post infection. As a result, mice in all groups showed relatively slight changes in body weight, with a reduction of less than 5% (Fig. 2E). Eltrombopag significantly reduced the viral copy numbers in the spleen and liver (Fig. 2F), in contrast, the other two compounds had no effect. Therefore, eltrombopag was identified as a promising candidate for further study.

Eltrombopag, especially administered via intraperitoneal injection, inhibits DENV 2 *in vivo*

Based on the pharmacological properties of eltrombopag described in previous reports (Lee et al., 2021), a set of animal experiments was designed to explore the efficacy of eltrombopag in DENV 2. Specifically, we measured indicators such as body weights, viral loads, and inflammatory cytokines after adjusting both the delivery dose and route (Fig. 3A). AG129 mice were administered with either 10 or 20 mg/kg eltrombopag via *i.g.* or *i.p.*, immediately after challenge with 1×10^7 $TCID_{50}$ of DENV 2 via *i.p.*, NITD008 administered via *i.g.* was used as a treatment control.

During the two-day period, the body weights of mice changed slightly in both the vehicle and treatment groups (Fig. 3B). According to the viral load results in Fig. 3C, eltrombopag reduced the viral copy numbers in the liver, spleen, and kidney in a dose-dependent manner, while exhibiting a stronger inhibitory effect when delivered via *i.p.* According to the inflammatory cytokines results, eltrombopag inhibited the expression of TNF-α and IL-6 in the blood (Fig. 3D), which was induced by DENV 2 infection. Accordingly, the pharmacokinetic data showed that eltrombopag administered via *i.p.* resulted in better absorption, distribution, and clearance than administration via *i.g.*, when taking *i.v.* administration as a reference (Fig. 3E). These results further confirmed the potential of eltrombopag in combating DENV 2.

Eltrombopag inhibits DENV 2 at the post-infection stage

To investigate the mechanism of action of eltrombopag on DENV 2, a set of time-of-addition experiments was performed to examine its effects on viruses and cells, which were treated as described in Fig. 4A. Eltrombopag exhibited comparable inhibition when added at the post-infection stage to that in the full-time treatment mode, but showed a negligible effect on the viruses and cells themselves (Fig. 4B). Furthermore, we added eltrombopag at 0, 2, 4, 6, 8, 12, 24, and 36 h after DENV 2 infection to confirm its effect at the post-infection stage (Fig. 4C). The addition of eltrombopag within 24 h following DENV 2 infection achieved effective inhibition, whereas addition at 36 h or later resulted in reduced inhibition. Ribavirin was effective within 12 h, thus working for a shorter time following infection (Fig. 4D). The same trend was observed in the images reflecting DENV 2 infection detected by IFA (Fig. 4E).

Eltrombopag allosterically binds to NS2B-NS3pro in a non-competitive manner

To reveal the mechanism of action of eltrombopag on NS2B-NS3pro, we validated the binding sites and mode involved. Through docking analysis on two separate confirmations representing the catalytic site (2FOM) and the allosteric site (6MO0), we predicted the binding sites on NS2B-NS3pro across the top nine most favorable conformations (Supplementary Table S1 and S2), then quantified the frequency of amino acid interactions with eltrombopag and listed them in order of their frequency of occurrence. We identified 26 amino acids around the catalytic pocket of DENV2 NS2B-NS3pro, which were likely to interact with eltrombopag, where one amino acid, H51, showed the highest frequency (>6) (Fig. 5A). Furthermore, we identified 17 amino acids around the allosteric pocket of DENV2 NS2B-NS3pro, which were likely to interact with eltrombopag, where L1085, L1076, H51, L1149, K1074, V1040, P1138, and N1167 showed the highest frequency (>6) (Fig. 5B).

Molecular dynamics simulations revealed that the binding of eltrombopag to 6MO0 is more stable than binding to 2FOM, reflected by minimal positional deviation (Fig. 5C). The 3D map of the free energy landscape also showed that the binding of eltrombopag to 6MO0 exhibits a nearly single and sharp minimum energy cluster, indicating a highly stable state (Fig. 5D). Through simulation-based calculations, the deductive binding capacity of eltrombopag to NS2B-NS3pro, as shown by both individual residue interactions (Fig. 5E) and integrated binding footprints (Table 2), demonstrated that the eltrombopag-6MO0 complex achieves a lower binding free energy. The 2D map of the free energy landscape revealed that eltrombopag binds to the "L" cavity of 6MO0 through interaction with the hot residues, at a minimum energy state (Fig. 5F). The above analysis together implied that eltrombopag preferentially binds the allosteric sites of NS2B-NS3pro.

To validate the deduction, a set of enzymatic kinetic experiments were performed by adjusting the concentrations of the enzyme, compound, or substrate. The results showed that eltrombopag reversibly binds to DENV2 NS2B-NS3pro, as indicated by straight lines passing through the origin and varying slopes corresponding to different compound concentrations (Fig. 5G). Furthermore, eltrombopag was shown to act in a substrate-non-competitive manner, as indicated by that Vmax changes with the concentrations of eltrombopag while the Km remains unchanged (Fig. 5H), consistent with the theoretical predictions. Hence, we concluded that eltrombopag allosterically binds to NS2B-NS3pro in a non-competitive manner to inhibit its activity.

Eltrombopag has a broad-spectrum effect on flaviviral NS2B-NS3 proteases

Because flaviviral NS2B-NS3pros have conservative protein sequences and structures (Fig. 6A and B), we analyzed the broad-spectrum effect of eltrombopag on four serotypes of DENV, namely DENV 1, DENV 2, DENV 3, and DENV 4, as well as the most closely related flavivirus,

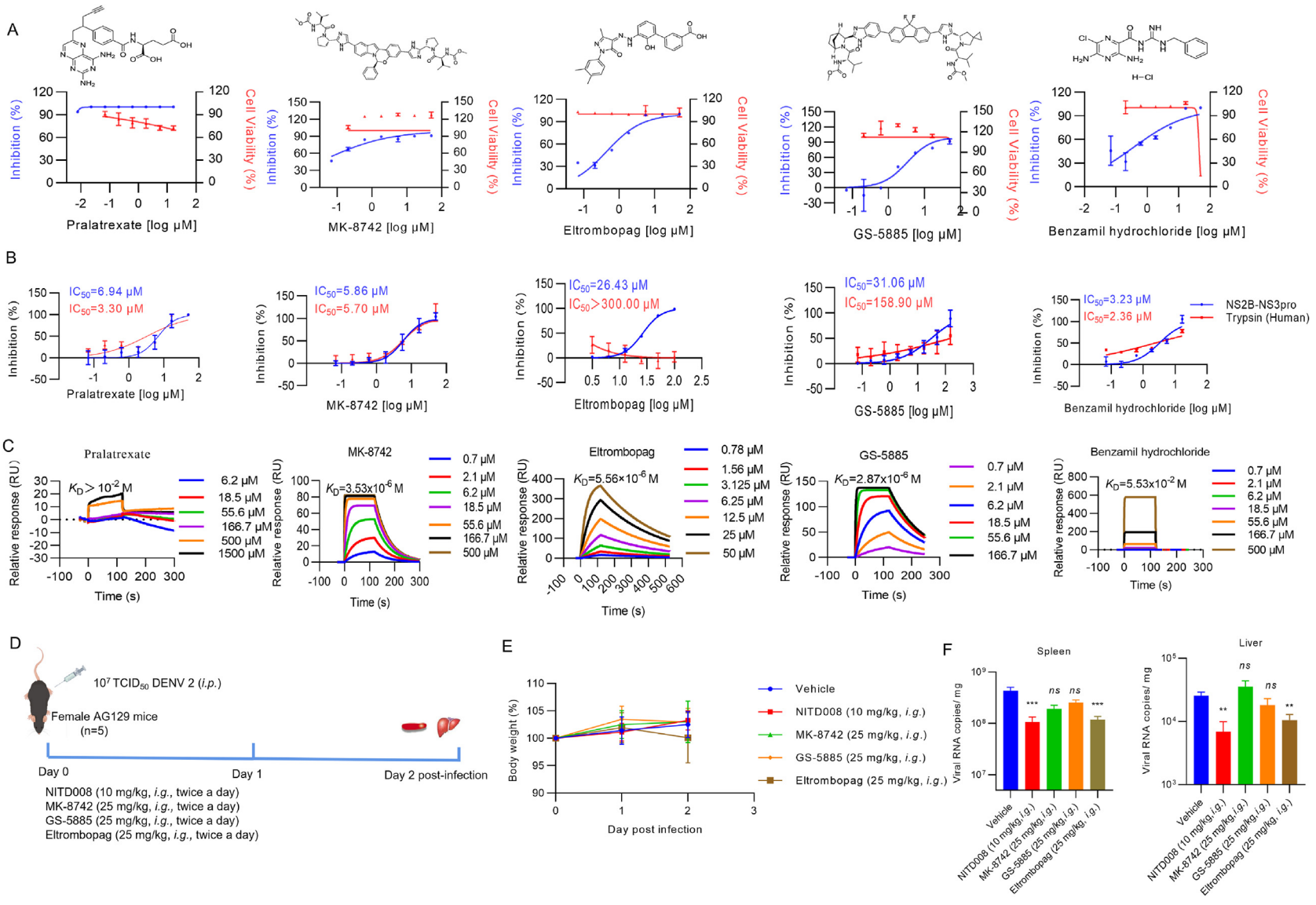

Fig. 2. Identification of eltrombopag as a promising candidate for DENV 2. **A** Dose-response curves of the antiviral activity and cytotoxicity of pralatrexate, MK-8742, eltrombopag, GS-5885, and benzamil hydrochloride on BHK-21 cells; chemical structures are shown with the curves. **B** Dose-dependent inhibition of pralatrexate, MK-8742, eltrombopag, GS-5885, and benzamil hydrochloride on NS2B-NS3pro and human trypsin detected by fluorescence resonance energy transfer assays. **C** Affinity of pralatrexate, MK-8742, eltrombopag, GS-5885, and benzamil hydrochloride analyzed by SPR; K_D values are shown with the curves. **D** Animal experimental scheme. Female AG129 mice (n = 5, 8–10 weeks old) were challenged with DENV 2 at a dose of 1×10^7 $TCID_{50}$ via intraperitoneal injection (*i.p.*), MK-8742, eltrombopag, GS-5885, and NITD008 were administered via intragavage (*i.g.*) **E** Body weights were recorded daily and plotted. **F** Viral copies in spleen and liver were measured by RT-qPCR two days post infection. *ns*, $P > 0.05$, $^{**}P < 0.01$, and $^{***}P < 0.001$ (Student's *t*-test, compared to vehicle).

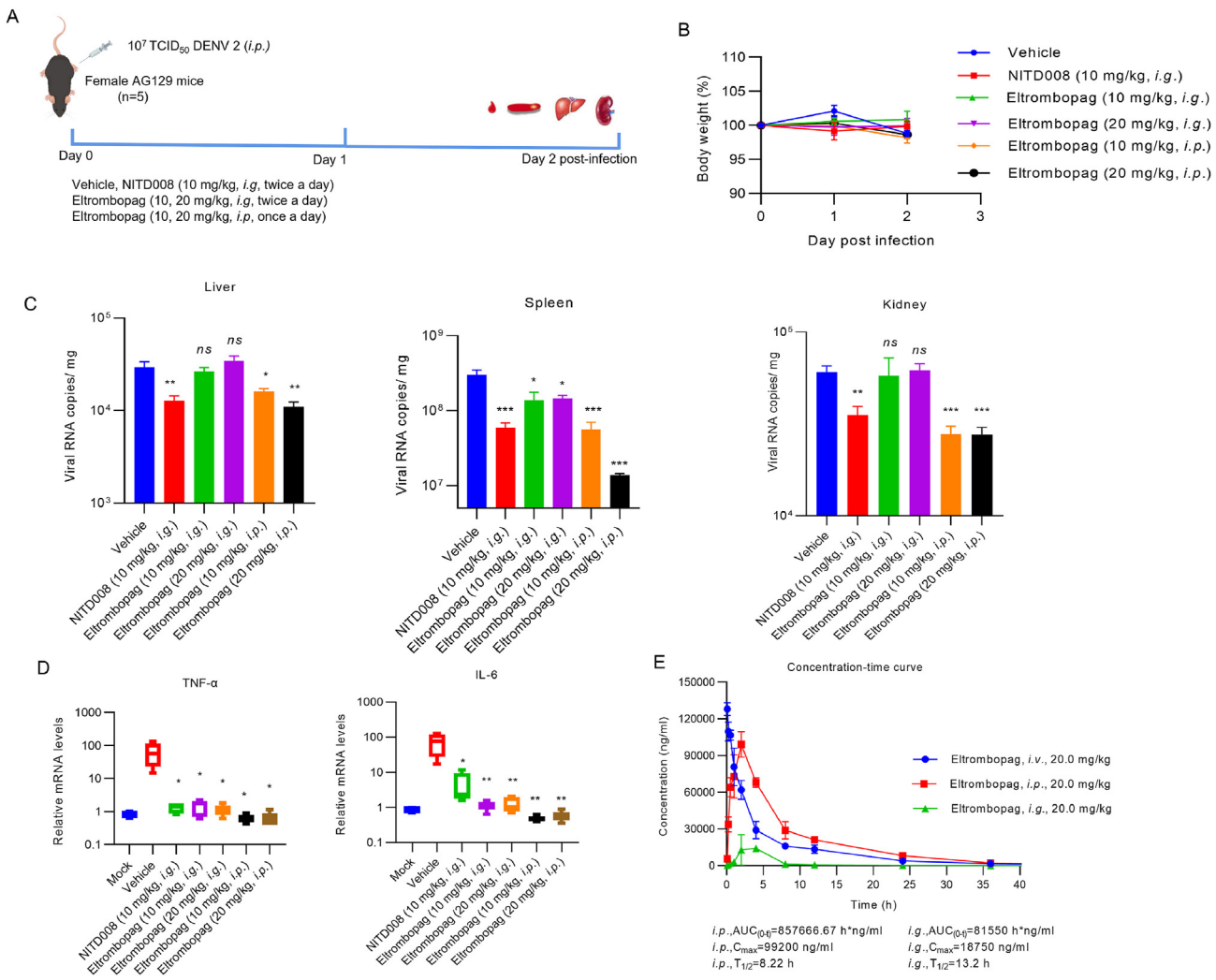

Fig. 3. *In vivo* antiviral effects of eltrombopag in AG129. **A** Animal experimental scheme. Female AG129 mice (n = 5, 8–10 weeks old) were treated with eltrombopag via intragavage (*i.g.*) or intraperitoneal injection (*i.p.*) after challenge of DENV 2 (1×10^7 $TCID_{50}$). Viral copies in the liver, spleen, and kidney, and inflammatory cytokines in blood were detected by RT-qPCR. **B** Mice body weights were recorded daily during the two-day experimental period. **C** Viral copies in the liver, spleen, and kidney were measured by RT-qPCR two days post challenge. **D** Expression of representative pro-inflammatory cytokines (TNF-α and IL-6) in the blood was measured by RT-qPCR. **E** Pharmacokinetic data was collected from SD rats with eltrombopag administration via *i.g.*, *i.p.*, or intravenous injection (*i.v.*) within 36 h. Concentration-time curves were plotted from at least eight time points and pharmacokinetic parameters were calculated and displayed. *ns*, $P > 0.05$, $^*P < 0.05$, $^{**}P < 0.01$, and $^{***}P < 0.001$ (Student's *t*-test, compared to vehicle).

ZIKV. Through a set of docking analyses on the binding of eltrombopag to the allosteric pocket, we determined the binding energies of eltrombopag to the NS2B-NS3pros of DENV 1, 2, 3, 4, and ZIKV as −8.9 kcal/mol, −10.5 kcal/mol, −8.7 kcal/mol, −8.8 kcal/mol, and −8.3 kcal/mol, respectively (Fig. 6C), implying its broad-spectrum binding to flaviviral NS2B-NS3pros. Based on the analysis results, we chose NS2B-NS3pros of DENV 4 and ZIKV for verification. Consequently, the IC_{50} values for eltrombopag against DENV 4 and ZIKV NS2B-NS3pros were 26.18 μM and 29.81 μM, respectively (Fig. 6D). These results collectively reveal the broad-spectrum antiviral effect of eltrombopag against flaviviruses and highlight its antiviral feasibility.

DISCUSSION

Diseases caused by flaviviral infections, especially those caused by DENV, remain a major global public health problem. The application of dengue vaccines is currently limited by the potential antibody or vaccine-dependent infection enhancement, and an effective and safe therapeutic agent against DENV is still lacking (World Health Organization, 2017; Wilder-Smith et al., 2019), highlighting the urgent need for candidate vaccines and therapeutics. Current strategies for DENV antiviral discovery mainly target NS2B-NS3, NS3, NS4B, and NS5. Among them, the NS2B-NS3 serine protease is considered a promising viral target because of its pivotal role in the cleavage of polyproteins during viral replication. Because the protease activity of NS3 requires the hydrophilic structural domain of NS2B to stabilize itself, NS2B has been identified as a co-factor of NS3 (Luo et al., 2015), and numerous compounds have been reported to target NS2B-NS3pro to exhibit antiviral effects against DENV or ZIKV (Wu et al., 2015; Zephyr et al., 2023). Despite this, no compounds have been approved in the clinic or proceeded to clinical trials, emphasizing the need to discover more candidates.

Repurposing compounds from FDA-approved drugs represents a labor-saving, economical, and rapid approach to discover new antiviral candidates, considering their safety and druggabilities. If an approved drug has additional efficacy in treating other diseases, its redevelopment is the quickest way to open new applications. In this study, we screened a library of 3273 FDA-listed and compendial compounds, five of which (pralatrexate, MK-8742, eltrombopag, GS-5885, and benzamil hydrochloride) exhibited good antiviral activity on DENV 2. Further investigation showed that eltrombopag, an FDA-approved thrombopoietin

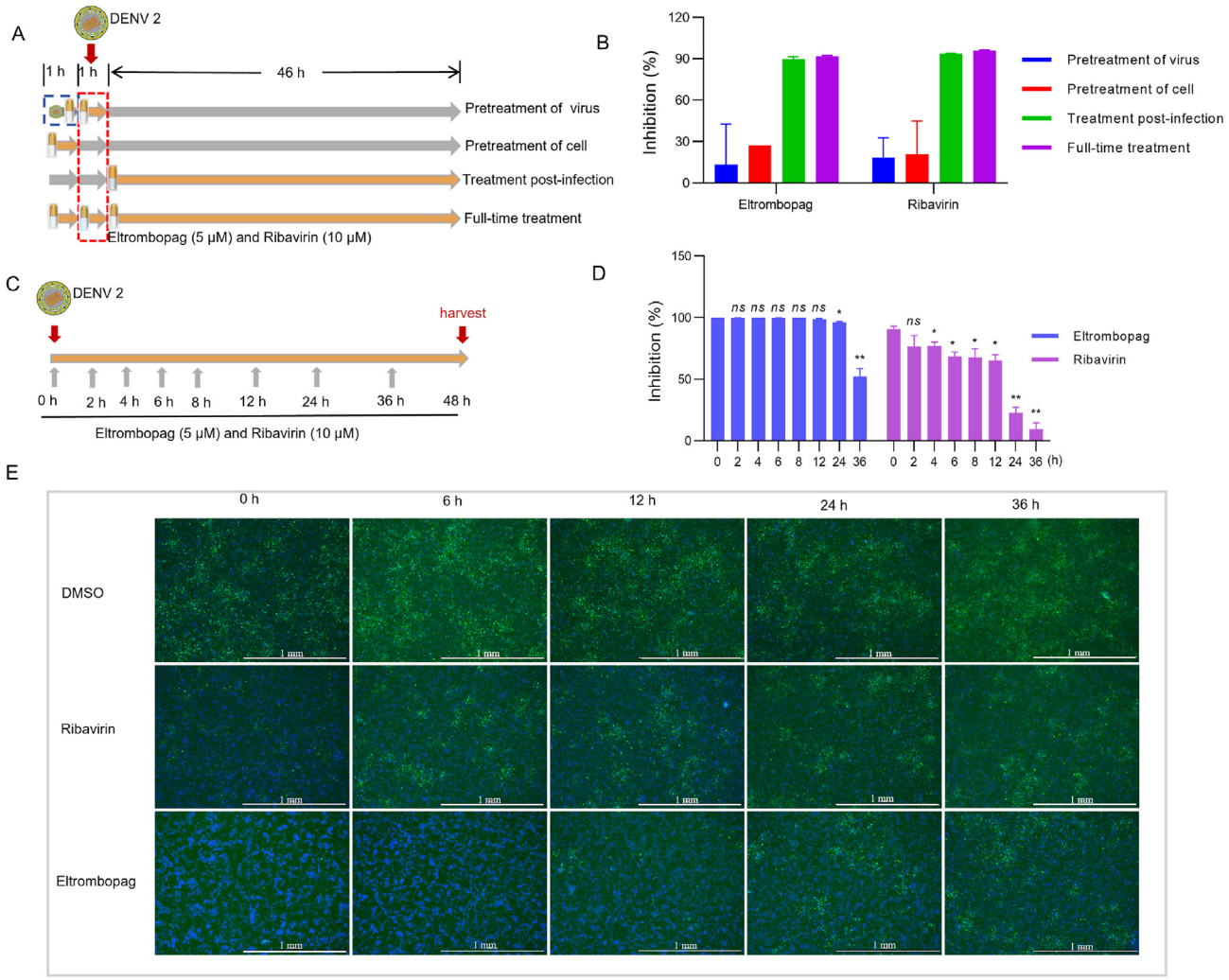

Fig. 4. Eltrombopag inhibits DENV 2 at the post-infection stage. **A** Schematic representation of the four treatment modes: pretreatment of virus, pretreatment of cell, post-infection treatment, and full-time treatment. **B** Inhibitory effect of eltrombopag on DENV 2 was examined by RT-qPCR at 48 h after applying the corresponding treatment mode; ribavirin was used as a control. **C** Schematic representation of the time-of-addition experiment with eltrombopag addition at 0, 2, 4, 6, 8, 12, 24, and 36 h post infection. **D** Inhibitory effect of eltrombopag on DENV 2 infection examined by RT-qPCR after 48 h; ribavirin was used as a control. **E** Indirect immunofluorescence assay (IFA) analysis of DENV 2 infection on BHK-21 cells after treatment with eltrombopag at different time points; DMSO served as a control. Bars represent 1 mm. *ns*, $P > 0.05$, $^{*}P < 0.05$, and $^{**}P < 0.01$ (Student's *t*-test, compared to 0 h).

receptor agonist and iron chelator that increases platelet counts in chronic immune thrombocytopenia (Zhang and Kolesar, 2011; Vlachodimitropoulou et al., 2017; Chakraborty et al., 2020), exhibits antiviral effects against DENV 2 infection both *in vitro* and *in vivo*. This study reported for the first time that eltrombopag manifests its antiviral effect by targeting NS2B-NS3pro. Furthermore, we revealed that eltrombopag reversibly binds to the allosteric sites rather than catalytic sites in a substrate non-competitive manner. Importantly, the allosteric pocket is conserved among DENV and ZIKV, explaining the broad-spectrum inhibition of eltrombopag on important flaviviruses. These results, in turn, emphasize the feasibility of targeting the NS2B-NS3pro allosteric site to discover flaviviral antivirals.

Using the repurposing strategy, temoporfin, clonidine, and nitazoxanide were previously screened from a total of 2816 approved and investigational drugs by Li et al., among which temoporfin was shown to bind ZIKV NS3 pockets that hold critical NS2B residues, thus inhibiting flaviviral polyprotein processing in a non-competitive manner (Li et al., 2017). Together with this study, our study proves the feasibility of repurposing candidates or lead compounds from the existing drugs. Notably, temoporfin also exhibits a broad-spectrum effect on flaviviruses; however, it targets sites distinct from the common catalytic sites targeted by orthosteric inhibitor such as erythrosin B (Li et al., 2018), functioning in a substrate non-competitive manner. Similar to the mechanism of temoporfin, eltrombopag, identified in our research, also bound to the allosteric sites to exhibit broad-spectrum inhibition. It is worth mentioning that allosteric inhibitors have an advantage in acting synergistically with the orthosteric inhibitors to reduce the risk of drug resistance (To et al., 2019), highlighting the promise of developing allosteric inhibitor such as eltrombopag.

Although eltrombopag is recommended as an oral medication for chronic immune thrombocytopenia in the clinic (Erickson-Miller et al., 2009), our study revealed better effects via intraperitoneal administration in animals, despite its oral bioactivity. In contrast to eltrombopag, MK-8742 and GS-5885 exhibited antiviral effects *in vitro* but not *in vivo*. This discrepancy may be attributed to their off-target effects *in vivo*. When compared with the human type abundant in gastric juice, only eltrombopag selectively inhibited NS2B-NS3 serine protease. Regardless, MK-8742 and GS-5885 exhibited favorable antiviral properties at both

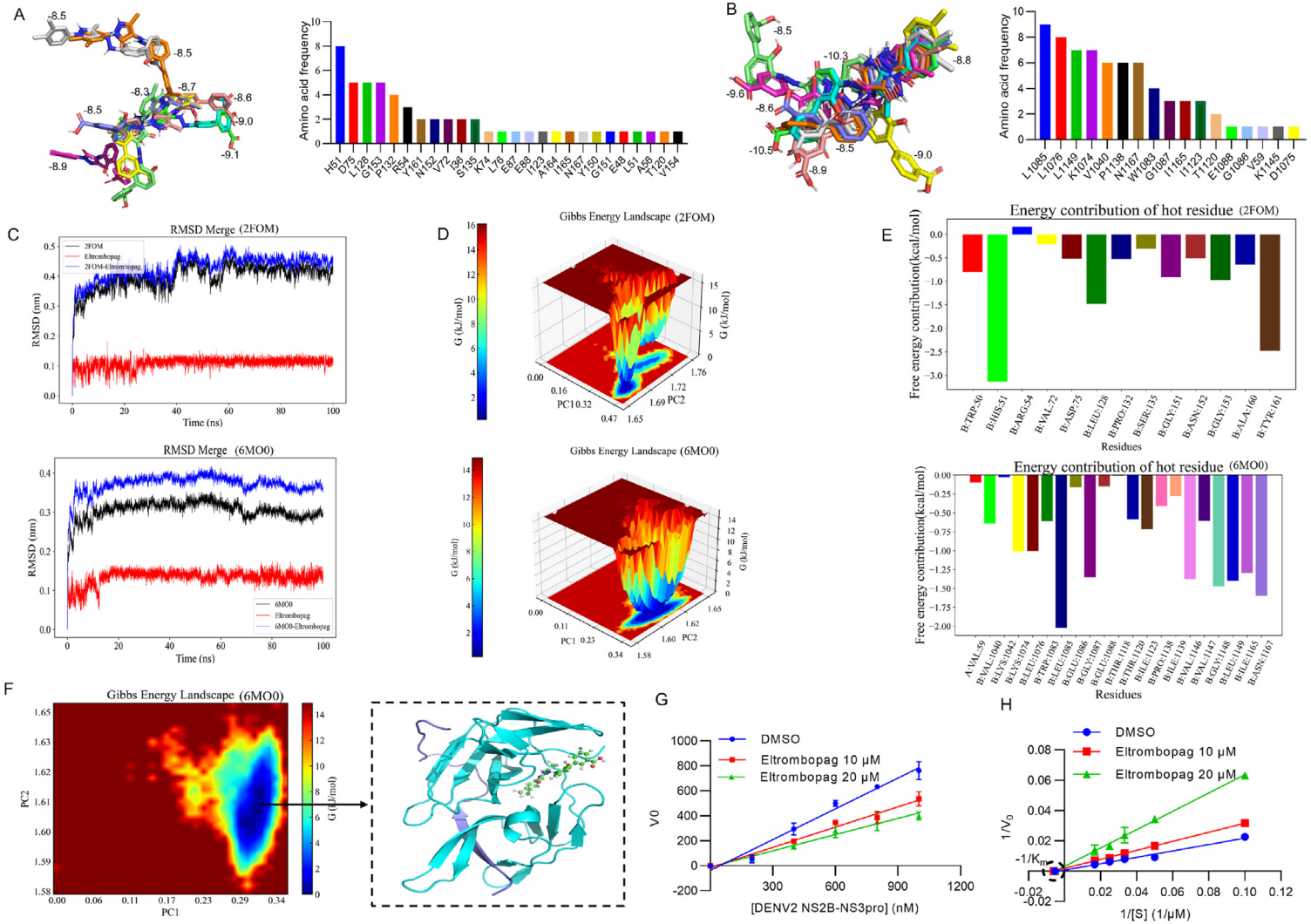

Fig. 5. Eltrombopag allosterically binds to NS2B-NS3pro. **A** and **B** Nine conformations by which eltrombopag binds to DENV 2 NS2B-NS3pro of 2FOM and 6MO0 were analyzed using Autodock Vina. Statistics of all amino acid residues from the nine conformations were plotted in order of their frequency of occurrence. **C** RMSD plots for eltrombopag only (red), 6MO0 or 2FOM only (black), and 6MO0 or 2FOM-eltrombopag complex (blue). **D** 3D Gibbs free energy landscape of the 2FOM-eltrombopag complex (upper) and 6MO0-eltrombopag complex (lower). **E** Energy contribution of the hot residues from either 2FOM (upper) or 6MO0 (lower). **F** The DENV 2 NS2B-NS3pro conformation at the low point of the 2D morphology of the 6MO0-eltrombopag complex. **G** The reaction rates of DENV 2 NS2B-NS3pro in a system with varying NS2B-NS3pro and fixed substrate concentrations. **H** Reaction rates of DENV 2 NS2B-NS3pro in a system with varying substrate and fixed NS2B-NS3pro concentrations.

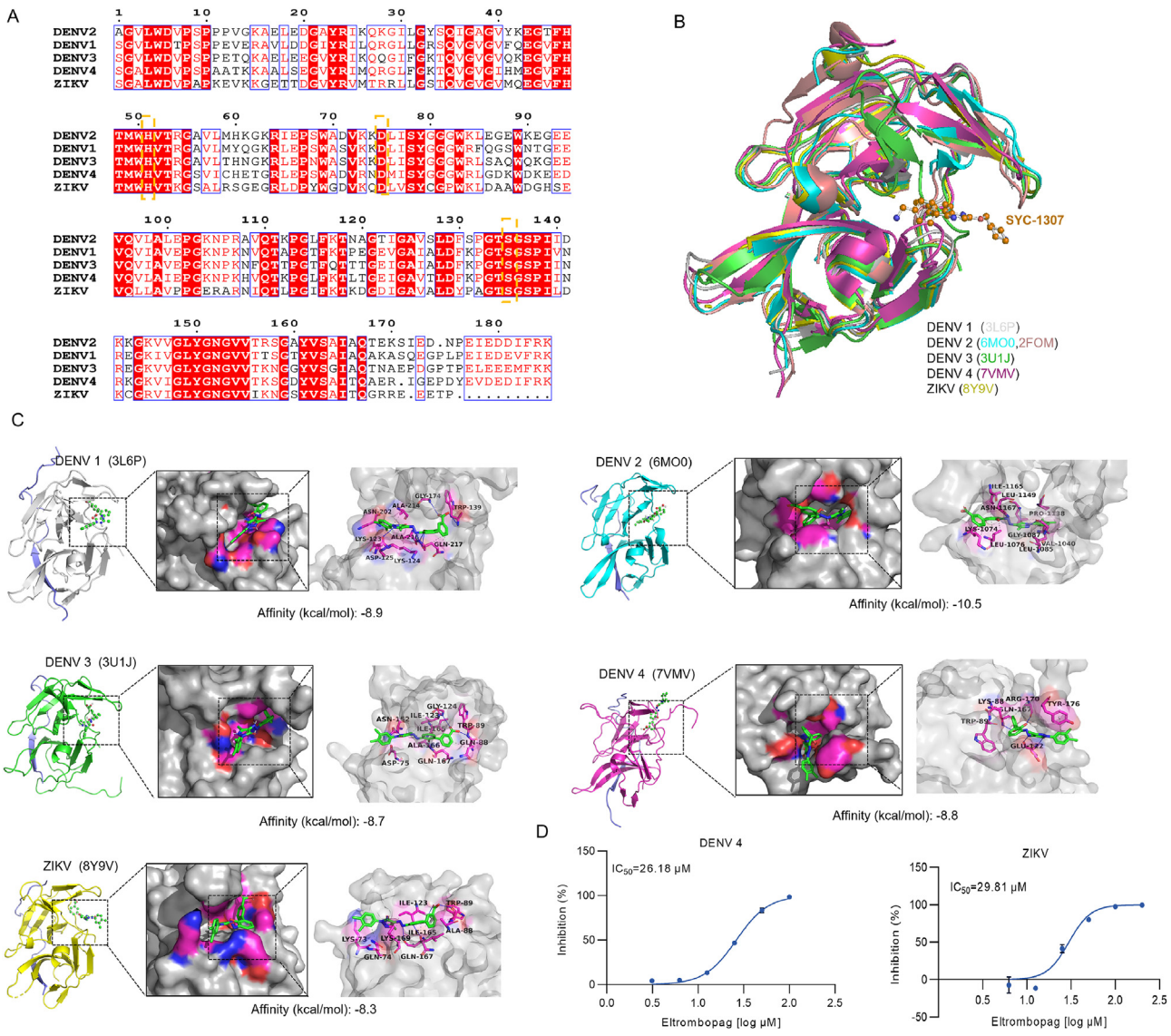

Fig. 6. Broad-spectrum effect of eltrombopag on flaviviral NS2B-NS3pros. **A** Conservative analysis on secondary structures of the NS3pros of DENV 1–4 and ZIKV. The catalytic triad is marked with yellow boxes. **B** Comparison on tertiary structures of the NS2B-NS3pros of DENV 1 (PDB: 3L6P, grizzly), DENV 2 (PDB: 6MO0, blue), DENV 3 (PDB: 3U1J, green), DENV 4 (PDB: 7VMV, purple), and ZIKV (PDB: 8Y9V, yellow), allosteric inhibitor (SYC-1307) exhibits a ball-and-stick structure. **C** Docking analysis of eltrombopag (green) with DENV 1 (PDB: 3L6P), DENV 2 (PDB: 6MO0), DENV 3 (PDB: 3U1J), DENV 4 (PDB: 7VMV), and ZIKV (PDB: 8Y9V). Calculated binding energies are also shown. Binding regions and sites are marked in pink and green, respectively. **D** Inhibition of the NS2B-NS3pro of DENV 4 and ZIKV by eltrombopag detected by FRET.

Table 2
Binding free energies of 2FOM/6MO0-eltrombopag complexes.

Contribution components	2FOM-Eltrombopag	6MO0-Eltrombopag
$\Delta_{VDWAALS}$	−45.95 ± 0.91	−49.37 ± 0.24
ΔE_{elec}	−23.84 ± 2.64	−31.27 ± 0.61
ΔE_{GB}	40.77 ± 0.70	50.08 ± 1.37
ΔE_{surf}	−4.16 ± 0.03	−6.32 ± 0.02
ΔG_{gas}	−69.79 ± 2.80	−80.64 ± 0.65
$\Delta G_{solvation}$	36.61 ± 0.70	43.75 ± 1.37
ΔTotal	−33.17 ± 2.88	−36.89 ± 1.52

the enzymatic and cellular levels, and molecular docking analysis suggested that these two compounds prefer to occupy the flat active pocket of NS2B-NS3pro because of their long-chain and symmetrical molecular structure (Supplementary Fig. S1). Further research should aim to improve their selectivities and affinities through chemical modifications based on structure-activity relationships.

Our study also preliminarily investigated the pharmacological properties of eltrombopag in terms of its administration dose, delivery route, and pharmacokinetics, and recommends a dose of no less than 10 mg/kg delivered via *i.p.*. Using a DENV 2-challenged AG129 mouse model that appears transient viremia lasting for several days, with viral load peaking at day 2 or 3 post-infection (Baldon et al., 2022), we observed eltrombopag decreases the viral loads in spleen by more than 1 log, after challenged with a dose of DENV 2 at 10^7 $TCID_{50}$. Importantly, eltrombopag is an FDA-approved drug for chronic immune thrombocytopenia, which works through agonizing the thrombopoietin receptor thus increases platelet counts, this may be helpful in clinical application of eltrombopag in DENV infection therapy, in view that thrombocytopenia is also a classical symptom of DENV infection. Nonetheless, eltrombopag should be evaluated with more models to better characterize its *in vivo* efficacy and safety.

This study also has some limitations. First, we did not sufficiently investigate the mechanism of action of eltrombopag; thus, further research should resolve the involved binding sites in more detail using X-ray crystallography. Moreover, eltrombopag is poorly water-soluble, which limits its applications for molecular biological analysis and *in vivo* dosage optimization. Future studies should make efforts to optimize its amphiphilicity, thus improving the bioavailability and *in vivo* efficacy before proceeding to formal preclinical development.

CONCLUSIONS

In summary, we developed a high-throughput screening system targeting NS2B-NS3 protease to identify compounds with antiviral effects against DENV 2, from an FDA-approved drug library. We identified eltrombopag and demonstrated its inhibitory effects against NS2B-NS3 protease and DENV 2 infection both *in vitro* and *in vivo*. This study revealed that eltrombopag reversibly binds to the allosteric sites of NS3 protease to exhibit broad-spectrum inhibitory effects against flaviviruses. This study repurposed an existing FDA-approved drug, eltrombopag, as a promising antiviral agent against DENV, providing an alternative for antiviral development against flaviviruses.

MATERIALS AND METHODS

Cells and viruses

BHK-21 and Huh 7 cells (ATCC, USA) were maintained in Dulbecco's modified Eagle's medium (DMEM, Gibco, USA) supplemented with 10% fetal bovine serum (Gibco, USA) and 1% antibiotic/antimycotic (Gibco, USA) at 37 °C in a humidified 5% CO_2 incubator. C6/36 cells (ATCC, USA) were maintained in Roswell Park Memorial Institute (RPMI-1640, Gibco, USA) supplemented with 10% fetal bovine serum and 1% antibiotic/antimycotic at 28 °C in a humidified 5% CO_2 incubator.

DENV 2 (*NGC*) was obtained from the School of Public Health and Tropical Medicine, Southern Medical University. DENV 2 was propagated with C6/36 cells.

Plasmid construction

The NS2B-NS3 sequences of DENV 2 (NC_001474.2), DENV 4 (NP_073286.1), and ZIKV (NC_012532.1) were synthesized by Sangon Biotech by adding a G4SG4 linker between NS2B (48–95 aa) and NS3 (1–185 aa).

Protein expression and purification

The expression and purification process of NS2B-NS3pro was performed as previously reported, with minor modifications (Wu et al., 2015). Briefly, the engineered bacteria, *E. coli* BL21(DE3) cells (Beyotime, China), were transformed with plasmids, and single clones were picked to inoculate in LB liquid medium containing 20 μg/mL of kanamycin. Once the OD600 reached 0.6−0.8, 1 mM isopropyl-β-D-thiogalactopyranose was added, followed by induction at 16 °C overnight. Subsequently, bacterial cells were collected by centrifugation at 12,000×*g* for 5 min at 4 °C, then suspended with lysis buffer (50 mM HEPES, 300 mM NaCl, and 5% glycerol, pH 7.5) and lysed by probe sonication on ice. Supernatants were collected by centrifugation at 12,000 ×*g* for 40 min at 4 °C, followed by HisTrap affinity chromatography (GenScript, USA). Finally, the eluents were detected for purity by Coomassie brilliant blue, and stored at −80 °C before use.

FRET assay

A high-throughput screening assay was established based on NS2B-NS3pro and measured by FRET, according to previous reports. Briefly, 10 μL of NS2B-NS3pro at a final concentration of 300 nM was mixed with 10 μL of the fluorophore-labeled peptide substrate, Bz-Nle-KRR-AMC (KKL, USA), at a final concentration of 20 μM in the reaction solution (200 mM Tris-HCl, pH 8.5). The reaction was monitored by detecting the fluorescence intensity on a microplate reader (BioTek) (λex/λem = 360 nm/460 nm) every 3 min for a total time of 30 min. Inhibition of NS2B-NS3pro activity by the compounds was calculated using the relative fluorescence units at saturation:

$$V{=}(F_2–F_1)/t,\ t = t_2\text{-}t_1 \quad (1)$$

where V is the enzyme reaction rate, t is the reaction duration, t_1 is the reaction starting time, t_2 is the reaction saturation time, F_1 is the fluorescence intensity at t_1, and F_2 is the fluorescence intensity at t_2:

$$\text{Inhibition } (\%) = 100\text{-}\ (V_{\text{experimental}}/V_{\text{control}}) \times 100 \quad (2)$$

High-throughput screening assay

A library of FDA and pharmacopoeia-listed compounds was purchased from MedChemExpress (MCE, China). The compounds were stored in DMSO at −80 °C before use. The 384-well reaction system for the enzyme activity assay was dispensed as follows: 1 μL of the compound at a final concentration of 50 μM was first mixed with 9 μL of NS2B-NS3pro at a final concentration of 300 nM, and incubated at 37 °C for 10 min. Then, 10 μL of the peptide substrate at a final concentration of 20 μM was added to reach a total volume of 20 μL. Subsequent procedures were the same as those for the FRET assay. DMSO was used as a negative control, and aprotinin (MCE, China) was used as a positive control.

Antiviral assay on cells

BHK-21 or Huh 7 cells were inoculated into 48-well cell culture plates at 4×10^4 cells/well and cultured at 37 °C in a 5% CO_2 incubator overnight. First, the compounds were diluted with DMEM containing 2% fetal bovine serum from an initial concentration of 50 μM with triple gradients; DMSO and ribavirin were used as the negative and positive control, respectively. After removing the cell supernatants, 200 μL of compound solution was added to the cells and incubated at 37 °C for 1 h. Then, 10 μL of viral dilution was added to each well at a multiplicity of infection of 1 (MOI = 1) and incubated with the cells at 37 °C for an additional 1 h. Subsequently, the inoculations were completely removed, and the cells were washed with PBS and incubated with the compound at the corresponding concentration. Two days later, the cell supernatants were collected for viral copy detection using real-time quantitative PCR (RT-qPCR), and the cells were fixed for immunofluorescence analysis.

Viral RNA was extracted using the DNA/RNA Extraction Kit (Vazyme, China) and detected using the HiScript II One Step qPCR SYBR Green Kit (Vazyme, China) according to the manufacturer's instructions. Copy numbers were calculated based on the standard curve method using a standard plasmid (DENV 2 NS5A, Sino Biological, China) and a pair of primers targeting DENV 2 NS5A (Supplementary Table S3).

Cytotoxicity assay

BHK-21 cells were seeded in 96-well plates overnight and treated with serially diluted hit compounds or DMSO for two days. Next, the culture medium containing the compounds was replaced with fresh medium containing the Cell Counting Kit-8 (CCK8) reagent (Vazyme, China). The cells were then incubated at 37 °C for an additional 2 h in the dark, and absorbance at OD450 was detected using a microplate reader (SYNERGY H1, BioTek, USA). DMSO (1%) was used as the control. Cell viability (%) was calculated as follows: $(OD_{\text{experimental group}}–OD_{\text{control group}})/OD_{\text{control group}} \times 100$.

Indirect immunofluorescence assay (IFA)

BHK-21 cells were fixed in 4% paraformaldehyde and permeabilized with 0.5% Triton X-100. Next, the cells were blocked with 5% nonfat milk and stained with primary anti-prM antibodies (Merck, Germany), followed by secondary goat anti-mouse Alexa Fluor-488 antibodies (Thermo Fisher Scientific, USA). The cell nuclei were stained with DAPI (Sigma-Aldrich, USA), and images were captured using a Cytation Image Reader (Bio-Rad, USA).

Surface plasmon resonance (SPR)

The binding affinity of pralatrexate, MK-8742, eltrombopag, GS-5885, and benzamil hydrochloride to NS2B-NS3pro recombinant proteins, evaluated by the equilibrium dissociation constant (K_D), was detected using an intermolecular interaction analysis system (Cytiva, USA). NS2B-NS3pro proteins were first immobilized on a CM5 microarray (Cytiva, USA) using a 1-ethyl-(3-dimethylaminopropyl) carbodiimide hydrochloride/N-hydroxysuccinimide-mediated cross-linking reaction. The compounds were serially diluted in PBS from an initial concentration of 1500 μM, 500 μM or 50 μM, then flowed over the chip at 30 μL/min for 120 s of association and 400 s of dissociation. Data were analyzed using Biacore evaluation software (version 1 K) fitted to a 1:1 binding model, and curves were drawn using GraphPad Prism 9.0.

Animal experiments

AG129 mice (female, 8–10 weeks old) were maintained in a specific pathogen-free animal facility and handled in an animal biosafety level 2 laboratory. Mice (n = 5 per group) were inoculated via intraperitoneal injection (*i.p.*) with 1×10^7 of the 50% tissue culture infectious dose ($TCID_{50}$) of DENV 2 and immediately administered the compounds via *i.p.* once a day or intragavage (*i.g.*) twice a day. The vehicle group was administered with the same volume of solvent (10% DMSO + 40% PEG300 + 5% Tween-80 + 45% saline), whereas the positive control group was administered with NITD008 at a dose of 10 mg/kg via *i.g.* twice a day. Mice were monitored for two days for body weight then sacrificed for blood, liver, spleen, and kidney harvesting. Tissues were collected for viral copy number or pro-inflammatory cytokines analysis.

Real-time qPCR for detecting viral copies and pro-inflammatory cytokines

The liver, spleen, and kidney tissues were weighed and homogenized in 1 mL of DMEM at 60 Hz for 45 s with 15 s-intervals for three times. Total RNA was extracted from 100 μL of homogenate or 100 μL of blood, according to the protocol of the RNeasy Mini Kit (Qiagen, Germany). The RT-qPCR procedures were similar to those used for the cellular antiviral assays. The viral copies and relative expression levels of pro-inflammatory cytokines were determined either by the standard curve method or $_{\Delta\Delta}$Ct method. Mouse ACTB was used as an internal reference gene; the primers for pro-inflammatory cytokines are listed in Supplementary Table S3.

Pharmacokinetics in rats

Male Sprague-Dawley rats (180–220 g) were randomly divided into three groups with three rats each. Before treatment, all rats were fasted overnight with free access to water or food. Eltrombopag was either suspended in 0.4% sodium carboxymethylcellulose and administered at a dose of 20 mg/kg via *i.g.,* or dissolved in solvent (10% DMSO, 40 % PEG 300, 5% Tween 80, 45% saline) with ultrasonication and administered via *i.p.* or intravenous injection (*i.v.*). Plasma samples were collected from the jugular veins at multiple time points within 36 h. Twenty-five microliters of plasma were mixed with an equal volume of diclofenac sodium and vortexed for 3 min, then 200 μL of acetonitrile were added and vortexed for 5 min. The mixture was centrifuged at 1700 ×*g* for 15 min at 4 °C, then 150 μL of supernatant were acquired and mixed with an equal volume of ultrapure water for liquid chromatography with tandem mass spectrometry. Pharmacokinetic parameters were calculated using WinNonlin software (version 8.3) by applying non-atrial modeling.

Time-of-addition assay

BHK-21 cells seeded overnight in 48-well plates were infected with DENV 2 (MOI = 0.1) for 1 h (0–1 h) in all groups. Four treatment modes were applied, using eltrombopag as the experimental compound and DMSO as a control: 1) pre-treatment of viruses (where viruses were pre-treated with compounds for 1 h and used to infect the cells); 2) pre-treatment of cells (−1–0 h); 3) post-infection treatment (1–46 h); and 4) full-time treatment (−1–46 h). The cells were infected with DENV 2 (MOI = 1) for 1 h, and the compounds were added at 0, 2, 4, 6, 8, 12, 24, and 36 h. After treatment, the cellular supernatants and cells were collected at 48 h for viral copy number detection using RT-qPCR or IFA.

Molecular docking analysis

The 3D structure spatial data files of the hit compounds were downloaded from PubChem (https://pubchem.ncbi.nlm.nih.gov/). Open Babel software was used to generate the PDBQT files of these ligands from the spatial data files. The NS2B-NS3pro structures of DENV 1 (PDB: 3L6P), DENV 2 (PDB: 2FOM), DENV 2 (PDB: 6MO0), DENV 3 (PDB: 3U1J), DENV 4 (PDB: 7VMV), and ZIKV (PDB: 8Y9V) were downloaded from the RCSB PDB (https://www.rcsb.org/). The AutoDock tool was used to convert these receptor structure files into PDBQT format. Molecular docking was performed using AutoDock Vina (v1.2.3) (Eberhardt et al., 2021). To identify lower-affinity binding sites, the grid box was set as a cube with a side-length parameter of 126. The binding sites identified by docking analysis were analyzed and visualized using the PLIP web tool (Adasme et al., 2021) and PyMOL, respectively.

Molecular dynamics simulation analysis (MD)

Gromacs 2022.3 software was used for molecular dynamics simulation analysis (Van Der Spoel et al., 2005; Abraham et al., 2015). For compound preprocessing, AmberTools22 was used to add the GAFF force field to eltrombopag, while Gaussian 16W was used to hydrogenate the compound and calculate the RESP potential. Potential data were added to the topology file of the molecular dynamics system. Simulation was conducted at constant temperature of 300 K and atmospheric pressure (1 Bar). The Amber99sb-ildn force field was used, with water as solvent (Tip3p water model). The total charge of the simulation system was neutralized by adding an appropriate number of Na + ions. The simulation system adopted the steepest descent method to minimize the energy, and then carried out the isothermal isovolumic ensemble (NVT) equilibrium and isothermal isobaric ensemble (NPT) equilibrium for 100,000 steps, with the coupling constant of 0.1 ps and the duration of 100 ps. Finally, free molecular dynamics simulation was performed. The process consisted of 5,000,000 steps, with a step length of 2 fs and total duration of 100 ns. After the simulation, the built-in tool of the software was used to analyze the trajectory, and the root-mean-square variance (RMSD), root-mean-square fluctuation (RMSF), and protein rotation radius of each amino acid trajectory were calculated, in combination with the free energy (MMGBSA), free energy topography, and other data.

Enzyme kinetic analysis

First, the initial reaction rate of DENV 2 NS2B-NS3pro in the presence of eltrombopag (0, 10 and 20 μM) at different concentrations (0, 200, 400, 600, 800 and 1000 nM) of NS2B-NS3pro was determined by fixing a constant concentration of Bz-Nle-KRR-AMC substrate (20 μM) in the reaction system. The correlation between enzyme concentration and

reaction rate was fitted using GraphPad Prism 9.0. Subsequently, the effect of eltrombopag at different concentrations (0, 10 and 20 μM) on the initial reaction rate of DENV 2 NS2B-NS3pro in the presence of Bz-Nle-KRR-AMC substrate at different concentrations (0, 10, 20, 30, 40 and 60 μM) was determined in a system where DENV 2 NS2B-NS3pro was fixed at a constant concentration of 300 nM. The correlation between substrate concentration and reaction rate was fitted using GraphPad Prism 9.0.

Data analysis

The data were processed using GraphPad Prism 9.0 software (CA, USA) and presented as the mean ± standard error of the mean (SEM). Statistical analyses included unpaired *t*-tests. The results were defined as *ns*, $P > 0.05$, $^{*}P < 0.05$, $^{**}P < 0.01$, or $^{***}P < 0.001$.

DATA AVAILABILITY

All data relevant to this study are included in the article or uploaded as supplementary information.

ETHICS STATEMENT

This study was approved by the Wuhan Institute of Virology, and the animal experiment protocols were approved by the Animal Ethics Committee (WIVA225202401).

AUTHOR CONTRIBUTIONS

Xuerui Zhu: investigation, data curation, validation & writing-original draft. Xiao Gao: methodology, data curation, validation. Yan Wu: methodology, project administration. Jia Lu: methodology, data curation. Xinlan Chen: methodology, data curation. Chenshu Zhao: formal analysis, methodology. Haoyu Li: methodology, software. Zhongfa Zhang: methodology, software. Shuwen Liu: funding acquisition, resources. Gengfu Xiao: supervision, validation. Xiaoyan Pan: conceptualization, supervision, writing-review & editing, validation.

CONFLICT OF INTEREST

Prof. Gengfu Xiao is the Editor-in-Chief for *Virologica Sinica* and was not involved in the editorial review or the decision to publish this article. All authors declare that there are no competing interests.

ACKNOWLEDGEMENTS

We are particularly grateful to the Institutional Center for Shared Technologies and Facilities of the Wuhan Institute of Virology, CAS, for their technical support. We also thank Prof. Xiaoguang Chen and Prof. Wei Zhao at the School of Public Health and Tropical Medicine, Southern Medical University, for providing the virus. This work was supported by the National Natural Science Foundation of China (Grant No. 82130101) and the Youth Innovation Promotion Association of CAS (Grant No. 2021333).

APPENDIX A. SUPPLEMENTARY DATA

Supplementary data to this article can be found online at https://doi.org/10.1016/j.virs.2025.05.009.

REFERENCES

Abraham, M.J., Murtola, T., Schulz, R., Páll, S., Smith, J.C., Hess, B., Lindahl, E., 2015. GROMACS: high performance molecular simulations through multi-level parallelism from laptops to supercomputers. SoftwareX 1–2, 19–25.

Adasme, M.F., Linnemann, K.L., Bolz, S.N., Kaiser, F., Salentin, S., Haupt, V.J., Schroeder, M., 2021. PLIP 2021: expanding the scope of the protein-ligand interaction profiler to DNA and RNA. Nucleic Acids Res. 49, W530–W534.

Baldon, L.V.R., de Mendonca, S.F., Ferreira, F.V., Rezende, F.O., Amadou, S.C.G., Leite, T., Rocha, M.N., Marques, J.T., Moreira, L.A., Ferreira, A.G.A., 2022. AG129 mice as a Comprehensive model for the experimental Assessment of mosquito Vector competence for Arboviruses. Pathogens 11, 879.

Bhatt, S., Gething, P.W., Brady, O.J., Messina, J.P., Farlow, A.W., Moyes, C.L., Drake, J.M., Brownstein, J.S., Hoen, A.G., Sankoh, O., Myers, M.F., George, D.B., Jaenisch, T., Wint, G.R., Simmons, C.P., Scott, T.W., Farrar, J.J., Hay, S.I., 2013. The global distribution and burden of dengue. Nature 496, 504–507.

Chakraborty, S., Alam, S., Sayem, M., Sanyal, M., Das, T., Saha, P., Sayem, M., Byapari, B.K., Tabassum, C.T., Kabir, A., Amin, M.R., Nabi, A., 2020. Investigation of the efficacy and safety of eltrombopag to correct thrombocytopenia in moderate to severe dengue patients - a phase II randomized controlled clinical trial. eClinicalMedicine 29–30, 100624.

Eberhardt, J., Santos-Martins, D., Tillack, A.F., Forli, S., 2021. AutoDock Vina 1.2.0: new docking methods, Expanded force field, and Python bindings. J. Chem. Inf. Model. 61, 3891–3898.

Erickson-Miller, C.L., Delorme, E., Tian, S.S., Hopson, C.B., Landis, A.J., Valoret, E.I., Sellers, T.S., Rosen, J., Miller, S.G., Luengo, J.I., Duffy, K.J., Jenkins, J.M., 2009. Preclinical activity of eltrombopag (SB-497115), an oral, nonpeptide thrombopoietin receptor agonist. Stem Cell. 27, 424–430.

Feng, Y., 2024. Recent advances in the study of zika virus structure, drug targets, and inhibitors. Front. Pharmacol. 15, 1418516.

Imperato, P.J., 2016. The Convergence of a virus, Mosquitoes, and human Travel in Globalizing the zika epidemic. J. Community Health 41, 674–679.

Katzelnick, L.C., Gresh, L., Halloran, M.E., Mercado, J.C., Kuan, G., Gordon, A., Balmaseda, A., Harris, E., 2017. Antibody-dependent enhancement of severe dengue disease in humans. Science 358, 929–932.

Lee, H., Lee, J., Hwang, J., Park, S., Kim, N., Kim, K., Lee, H., Shum, D., Jang, S., 2021. Repurposing eltrombopag for Multidrug resistant Staphylococcus aureus infections. Antibiotics (Basel) 10, 1372.

Li, Z., Brecher, M., Deng, Y.Q., Zhang, J., Sakamuru, S., Liu, B., Huang, R., Koetzner, C.A., Allen, C.A., Jones, S.A., Chen, H., Zhang, N.N., Tian, M., Gao, F., Lin, Q., Banavali, N., Zhou, J., Boles, N., Xia, M., Kramer, L.D., Qin, C.F., Li, H., 2017. Existing drugs as broad-spectrum and potent inhibitors for Zika virus by targeting NS2B-NS3 interaction. Cell Res. 27, 1046–1064.

Li, Z., Sakamuru, S., Huang, R., Brecher, M., Koetzner, C.A., Zhang, J., Chen, H., Qin, C.F., Zhang, Q.Y., Zhou, J., Kramer, L.D., Xia, M., Li, H., 2018. Erythrosin B is a potent and broad-spectrum orthosteric inhibitor of the flavivirus NS2B-NS3 protease. Antivir. Res. 150, 217–225.

Lim, S.P., 2019. Dengue drug discovery: Progress, challenges and outlook. Antivir. Res. 163, 156–178.

Luo, D., Vasudevan, S.G., Lescar, J., 2015. The flavivirus NS2B-NS3 protease-helicase as a target for antiviral drug development. Antivir. Res. 118, 148–158.

Messina, J.P., Brady, O.J., Golding, N., Kraemer, M.U.G., Wint, G.R.W., Ray, S.E., Pigott, D.M., Shearer, F.M., Johnson, K., Earl, L., Marczak, L.B., Shirude, S., Davis Weaver, N., Gilbert, M., Velayudhan, R., Jones, P., Jaenisch, T., Scott, T.W., Reiner Jr., R.C., Hay, S.I., 2019. The current and future global distribution and population at risk of dengue. Nat. Microbiol. 4, 1508–1515.

Murray, N.E., Quam, M.B., Wilder-Smith, A., 2013. Epidemiology of dengue: past, present and future prospects. Clin. Epidemiol. 5, 299–309.

Narayan, R., Tripathi, S., 2020. Intrinsic ADE: the dark side of antibody dependent enhancement during dengue infection. Front. Cell. Infect. Microbiol. 10, 580096.

Niu, C., Huang, Y., Wang, M., Huang, D., Li, J., Huang, S., Yang, F., Wan, C., Zhang, R., 2020. Differences in the Transmission of dengue fever by different serotypes of dengue virus. Vector Borne Zoonotic Dis. 20, 143–150.

Patkar, C.G., Kuhn, R.J., 2008. Yellow Fever virus NS3 plays an essential role in virus assembly independent of its known enzymatic functions. J. Virol. 82, 3342–3352.

Paz-Bailey, G., Adams, L.E., Deen, J., Anderson, K.B., Katzelnick, L.C., 2024. Dengue. Lancet 403, 667–682.

Rice, C.M., Lenches, E.M., Eddy, S.R., Shin, S.J., Sheets, R.L., Strauss, J.H., 1985. Nucleotide sequence of yellow fever virus: implications for flavivirus gene expression and evolution. Science 229, 726–733.

Saron, W.A.A., Shanmugam, K., Tung, C.C., Patmanathan, R.K., Rathore, A.P.S., Anderson, D.E., St John, A.L., 2023. Exacerbated Zika virus-induced neuropathology and microcephaly in fetuses of dengue-immune nonhuman primates. Sci. Transl. Med. 15, eadd2420.

Shukla, S., Hong, S.Y., Chung, S.H., Kim, M., 2016. Rapid detection strategies for the global threat of zika virus: current state, new Hypotheses, and limitations. Front. Microbiol. 7, 1685.

Starvaggi, J., Previti, S., Zappala, M., Ettari, R., 2024. The inhibition of NS2B/NS3 protease: a new therapeutic Opportunity to Treat dengue and zika virus infection. Int. J. Mol. Sci. 25, 4376.

To, C., Jang, J., Chen, T., Park, E., Mushajiang, M., De Clercq, D.J.H., Xu, M., Wang, S., Cameron, M.D., Heppner, D.E., Shin, B.H., Gero, T.W., Yang, A., Dahlberg, S.E., Wong, K.K., Eck, M.J., Gray, N.S., Janne, P.A., 2019. Single and dual targeting of Mutant EGFR with an allosteric inhibitor. Cancer Discov. 9, 926–943.

Van Der Spoel, D., Lindahl, E., Hess, B., Groenhof, G., Mark, A.E., Berendsen, H.J., 2005. GROMACS: fast, flexible, and free. J. Comput. Chem. 26, 1701–1718.

Vlachodimitropoulou, E., Chen, Y.L., Garbowski, M., Koonyosying, P., Psaila, B., Sola-Visner, M., Cooper, N., Hider, R., Porter, J., 2017. Eltrombopag: a powerful chelator of cellular or extracellular iron(III) alone or combined with a second chelator. Blood 130, 1923–1933.

Weaver, S.C., Reisen, W.K., 2010. Present and future arboviral threats. Antivir. Res. 85, 328–345.
Wilder-Smith, A., Hombach, J., Ferguson, N., Selgelid, M., O'Brien, K., Vannice, K., Barrett, A., Ferdinand, E., Flasche, S., Guzman, M., Novaes, H.M., Ng, L.C., Smith, P.G., Tharmaphornpilas, P., Yoon, I.K., Cravioto, A., Farrar, J., Nolan, T.M., 2019. Deliberations of the strategic Advisory group of Experts on Immunization on the use of CYD-TDV dengue vaccine. Lancet Infect. Dis. 19, e31–e38.
World Health Organization, 2017. Dengue vaccine: WHO position paper, July 2016 - recommendations. Vaccine 35, 1200–1201.
Wu, D.W., Mao, F., Ye, Y., Li, J., Xu, C.L., Luo, X.M., Chen, J., Shen, X., 2015. Policresulen, a novel NS2B/NS3 protease inhibitor, effectively inhibits the replication of DENV2 virus in BHK-21 cells. Acta Pharmacol. Sin. 36, 1126–1136.
Zephyr, J., Rao, D.N., Johnson, C., Shaqra, A.M., Nalivaika, E.A., Jordan, A., Kurt Yilmaz, N., Ali, A., Schiffer, C.A., 2023. Allosteric quinoxaline-based inhibitors of the flavivirus NS2B/NS3 protease. Bioorg. Chem. 131, 106269.
Zhang, Y., Kolesar, J.M., 2011. Eltrombopag: an oral thrombopoietin receptor agonist for the treatment of idiopathic thrombocytopenic purpura. Clin. Ther. 33, 1560–1576.